AIMS Mathematics, 10(11): 27412–27439.
DOI: 10.3934/math.20251205
Received: 11 September 2025
Revised: 23 October 2025
Accepted: 11 November 2025
Published: 25 November 2025

http://www.aimspress.com/journal/Math

Theory article

A novel SIR-based computer virus propagation model with Beddington-DeAngelis functional response: Stability analysis and practical implications

Honglei Lu[1] **and Erxi Zhu**[2,*]

[1] College of Internet of Things Engineering, Jiangsu Vocational College of Information Technology, No.1 qianou Road, Huishan District, Wuxi 214153, Jiangsu, China

[2] College of Information Engineering, Changzhou Vocational Institute of Industrial Technology, No. 28, Mingxin Middle Road, Wujin District, Changzhou 213164, Jiangsu, China

* **Correspondence:** Email: erxi666@163.com.

Abstract: Understanding the dynamics of the propagation of computer viruses is crucial for the development of effective cybersecurity strategies. This paper proposes a novel compartmental model based on the traditional SIR framework, which incorporats the Beddington-DeAngelis functional response to capture the inhibitory effects of the modern operating systems' built-in security mechanisms. We rigorously establish the well-posedness of the model by proving the non-negativity and boundedness of solutions. The existence and stability of equilibrium points are thoroughly analyzed using the Hurwitz criterion, Lyapunov functions, and Dulac criterion. Numerical simulations validate our theoretical findings and demonstrate the significant role of the system self-protection parameters in controlling virus spread. Unlike previous models, our approach provides explicit connections between the model parameters and real-world cybersecurity metrics, thus offering practical insights for network defense strategies. The model's ability to maintain a persistent infected state aligns with the observed behaviors of modern malware, thus providing a more realistic representation of the dynamics of computer viruses. The study employs advanced visualization techniques, including three-dimensional surface plots to elucidate the complex interactions between protection parameters, thus providing actionable insights for the design and implementation of cybersecurity policies.

Keywords: computer virus propagation; SIR model; Beddington-DeAngelis functional response; global stability; Lyapunov function; cybersecurity
Mathematics Subject Classification: 68M12, 93A30

1. Introduction

Cybersecurity has emerged as a critical global concern in the digital age [1, 2]. Computer viruses, worms, and other malicious software continue to cause substantial financial losses and operational disruptions worldwide [3, 4]. The rapid evolution of communication technologies and the internet's infrastructure have facilitated the emergence of increasingly sophisticated malware variants, ranging from traditional email-borne viruses to contemporary ransomware, cryptojackers, and advanced persistent threats.

Traditional approaches to virus mitigation, primarily based on signature detection and reactive patching, suffer from fundamental limitations. Antivirus software typically requires the identification of a threat before developing countermeasures, thus creating a vulnerability window during the critical early stages of an outbreak [5]. This challenge is compounded by the continuous emergence of novel malware strains with diverse propagation mechanisms, which often evade conventional detection methods.

Mathematical modeling approaches, inspired by epidemiological studies of infectious diseases [6], have provided valuable information on the dynamics of virus propagation. Based on infection mechanisms and network interactions, various compartmental models have been developed, including SI, SIS [7], SIR [8], SIRS [9], and more complex variants [10,11]. Recent research has further extended these models to incorporate network topology considerations [12], fractional calculus approaches [13], and stochastic elements [14].

Despite these advances, a significant limitation persists for the most existing compartmental models for computer viruses: the treatment of system defense mechanisms is often oversimplified. Many models incorporate nonlinear incidence rates, such as the Holling Type-II functional response $\frac{\beta SI}{1+\sigma_1 S}$, to capture the saturation effect of the infection force [15]. While this represents a step forward, it primarily models the innate, static protection of systems (e.g., baseline firewall configurations, port security), which reduces the effective infection rate as the number of hardened (S) devices increases. Crucially, these models fail to capture the adaptive, dynamic response of modern cybersecurity systems that activate and intensify upon detecting malicious activity within the network.

Furthermore, recent research continues to advance the sophistication of epidemic-type models. For example, a stability analysis of nonlinear systems with various functional responses and time delays remains an active area of investigation, thus reflecting the complex and often delayed dynamics inherent in real-world propagation phenomena [16]. Studies such as [16] demonstrate rigorous analytical techniques to establish global stability in high-dimensional nonlinear systems, which share methodological parallels with our stability analysis. While their focus may be on biological epidemics, the underlying mathematical principles regarding the construction of Lyapunov functions and the handling of nonlinear incidence rates are directly relevant to our work. Our model contributes to this ongoing discourse by introducing and rigorously analyzing the Beddington-DeAngelis(B-D) functional response within the specific and critically important context of computer virus propagation, a domain where such advanced functional responses have been underexplored.

To address this gap, this paper introduces a novel SIR-based model that incorporates the B-D functional response. The key innovation of this choice lies in its two-parameter saturation structure, $\frac{\beta SI}{1+\sigma_1 S+\sigma_2 I}$. This form allows the model to decouple and independently represent two distinct phases of cyber defense:

- Innate protection (σ_1): The term $\sigma_1 S$ captures the saturation effect from susceptible devices, thus representing pre-existing static security measures such as firewall rules, access control lists, and system hardening.
- Adaptive response (σ_2): The novel introduction of the term $\sigma_2 I$ models the inhibitory effect of the infected population itself. This represents dynamic defense mechanisms, such as intrusion detection systems (IDS), security information and event management (SIEM) systems, endpoint detection and response (EDR), and network traffic analyses, that are triggered by the prevalence of an attack (I), which lead to increased network-wide vigilance, patch deployment, and isolation of compromised nodes, thus further reducing the virus propagation efficiency.

Unlike the Holling Type-II response, the B-D form can model the reality that a network's defense strengthens in response to an ongoing infection, thus providing a more nuanced and realistic representation of modern cybersecurity environments where both preventive and reactive controls are essential. This dual-parameter approach enables our model to provide specific insights into the relative effectiveness of prevention-focused versus response-focused security strategies.

2. Model formulation and preliminaries

2.1. Model assumptions and structure

We consider a computer network where each node represents a computer that can exist in one of three states [17]:

(1) Susceptible (S): Computers vulnerable to infection;
(2) Infected (I): Computers that are infected and can spread the virus; and
(3) Recovered (R): Computers that have been cured and have gained temporary immunity, typically through the installation of a specific antivirus signature or patch that targets the current virus strain.

The model incorporates the following biological and technological realities [18]:

(1) Modern operating systems have built-in protection mechanisms that resist virus propagation.
(2) Infected computers can be disinfected through an antivirus treatment.
(3) Recovered computers may lose immunity over time. This critical assumption models the reality that the specific protection (e.g., a virus signature or a software patch) can become obsolete. This obsolescence primarily occurs due to two interconnected factors:

    - Software Updates: Major operating system or application updates can alter the system's underlying code structure, thus potentially invalidating the previous patches or creating new, unforeseen vulnerabilities that the old protection does not cover.
    - Discovery of New Vulnerabilities: The continuous discovery of new zero-day vulnerabilities or novel attack techniques (e.g., polymorphic or metamorphic code) can render the existing signature-based immunity ineffective against new virus variants.

(1) Computers enter and leave the network through various means.

2.2. Mathematical formulation

The proposed model extends the traditional SIR framework by incorporating a B-D functional response as follows:

$$\begin{cases} \frac{dS}{dt} = (1-p)b - \frac{\beta S I}{1+\sigma_1 S+\sigma_2 I} - dS + \delta R, \\ \frac{dI}{dt} = \frac{\beta S I}{1+\sigma_1 S+\sigma_2 I} - (d+\alpha+\gamma)I, \\ \frac{dR}{dt} = \gamma I + pb - (d+\delta)R, \end{cases} \tag{2.1}$$

with the initial conditions $S(0) \geq 0$, $I(0) \geq 0$, $R(0) \geq 0$.

The parameters are defined as follows:

- b: Recruitment rate of new computers into the network.
- p: Proportion of new computers with pre-installed immunity.
- β: Effective infection rate.
- d: Removal rate of computers due to obsolescence or failure.
- α: Virus-induced failure rate.
- γ: Recovery rate of infected computers.
- δ: Rate of immunity loss. This parameter quantifies the rate at which a recovered computer transitions back to the susceptible state. Its value is determined by the dynamic cybersecurity environment. We propose that δ can be conceptually linked to practical operational metrics through the following relationship:

$$\delta \approx \lambda_v + \lambda_u \cdot (1-\eta_p), \tag{2.2}$$

  where:

  – λ_v represents the rate of discovery of new, relevant vulnerabilities that can bypass existing defenses.
  – λ_u represents the frequency of major software updates that potentially alter the system environment.
  – η_p represents the efficiency of the patch management process (i.e., the probability that a new patch (conferring renewed immunity) is applied before the computer is exposed to a new threat). A highly efficient process ($\eta_p \to 1$) can mitigate the immunity loss caused by software updates.

  Therefore, a high vulnerability discovery rate (λ_v), frequent software updates (λ_u), and an inefficient patching process ($\eta_p \ll 1$) all contribute to a higher effective immunity loss rate δ, thus making the network more susceptible to re-infection. This framework allows for a more nuanced interpretation of δ beyond a simple constant, thereby directly connecting it to key aspects of cybersecurity operational management.
- σ_1, σ_2: Saturation parameters that quantify the protection strength of the system.

The term $\frac{\beta S I}{1+\sigma_1 S+\sigma_2 I}$ represents the B-D functional response. This formulation is pivotal to our model's novelty, as it generalizes several common incidence forms and provides a flexible framework to quantify the inhibitory effects of system protection mechanisms in computer networks.

- Generalization Capability: The B-D functional response encompasses several classical incidence forms as special cases:

  - When $\sigma_2 = 0$, it reduces to the Holling Type-II response, thus only modeling only the saturation effect from susceptible devices (innate protection only).
  - When $\sigma_1 = 0$, it represents a scenario where protection is purely reactive and scales with the observed infection level.
  - When both $\sigma_1 = 0$ and $\sigma_2 = 0$, it simplifies to the bilinear incidence rate used in basic SIR models.

- Dual-Phase Defense Modeling: The simultaneous presence of both σ_1 and σ_2 enables our model to capture the synergistic interaction between innate and adaptive defenses. The parameter σ_1 (innate protection) quantifies the strength of the baseline security configurations (e.g., default-deny policies, system hardening, regular patching). In contrast, the parameter σ_2 (adaptive response) quantifies the efficacy of threat-induced countermeasures (e.g., the sensitivity of an IDS, the effectiveness of automated isolation protocols, the speed of security patch deployment).

This mathematical structure provides a more realistic representation of contemporary cybersecurity environments, where organizations implement layered defense strategies by combining both preventive controls (σ_1) and detective/responsive controls (σ_2). The decoupling of these two protection mechanisms allows for a more detailed analysis of cybersecurity investment strategies, thereby directly linking the model parameters to actionable security decisions and budget allocations.

The B-D functional response generalizes several classical incidence forms.

- If $\sigma_2 = 0$, then it reduces to the Holling type-II response, which only accounts for susceptible saturation.
- If $\sigma_1 = 0$, then it becomes a saturation function of infected hosts, thus reflecting reactive defenses.
- The simultaneous presence of both σ_1 and σ_2 enables the model to capture the synergistic effect of innate and adaptive protections, thus providing a more flexible and realistic representation of modern cybersecurity dynamics.

3. Mathematical analysis

3.1. Positivity and boundedness

Theorem 3.1 (Non-negativity and boundedness)**.** *For any non-negative initial conditions* $(S(0), I(0), R(0)) \in \mathbb{R}^3_+$*, the solutions of system (2.1) remain non-negative for all* $t \geq 0$ *and are uniformly ultimately bounded in the region.*

$$\Omega = \left\{(S, I, R) \in \mathbb{R}^3_+ : S + I + R \leq \frac{b}{d}\right\}. \tag{3.1}$$

Proof. To prove non-negativity, consider the first equation of system (2.1):

$$\frac{dS}{dt} \geq -\left(\frac{\beta I}{1 + \sigma_1 S + \sigma_2 I} + d\right) S.$$

This implies that

$$S(t) \geq S(0) \exp\left(-\int_0^t \left(\frac{\beta I(\tau)}{1 + \sigma_1 S(\tau) + \sigma_2 I(\tau)} + d\right) d\tau\right) \geq 0.$$

Similar arguments apply to $I(t)$ and $R(t)$, thus establishing non-negativity.

For boundedness, let $N(t) = S(t) + I(t) + R(t)$. Then,

$$\frac{dN}{dt} = b - dN - \alpha I \leq b - dN.$$

Solving this differential inequality yields the following:

$$N(t) \leq \frac{b}{d} + \left(N(0) - \frac{b}{d}\right)e^{-dt}.$$

Thus, $\limsup_{t\to\infty} N(t) \leq \frac{b}{d}$, which proves ultimate boundedness. □

3.2. Well-posedness and invariant region

The following lemma establishes that the region Ω is positively invariant, which is crucial to the biological significance of our model.

Lemma 3.1. *The region* $\Omega = \left\{(S, I, R) \in \mathbb{R}^3_+ : S + I + R \leq \frac{b}{d}\right\}$ *is positively invariant for system* (2.1).

Proof. From Theorem 3.1, we have $\frac{dN}{dt} \leq b - dN$. Consider the function $V(t) = N(t) - \frac{b}{d}$. Then,

$$\frac{dV}{dt} = \frac{dN}{dt} \leq -d\left(N - \frac{b}{d}\right) = -dV(t).$$

This implies $V(t) \leq V(0)e^{-dt}$. If $N(0) \leq \frac{b}{d}$, then $V(0) \leq 0$, and consequently $V(t) \leq 0$ for all $t \geq 0$, that is, $N(t) \leq \frac{b}{d}$ for all $t \geq 0$. Thus, Ω is positively invariant. □

3.3. Existence of equilibrium points

System (2.1) has two types of equilibrium points: the virus-free equilibrium E_0 and the endemic equilibrium E^*.

The virus-free equilibrium is given by the following.

$$E_0 = (S_0, I_0, R_0) = \left(\frac{(1-p)b}{d} + \frac{\delta pb}{d(d+\delta)}, 0, \frac{pb}{d+\delta}\right).$$

The basic reproduction number R_0 is obtained by using the next generation matrix method as follows.

$$R_0 = \frac{\beta S_0}{(d+\alpha+\gamma)(1+\sigma_1 S_0)}.$$

The endemic equilibrium $E^* = (S^*, I^*, R^*)$ satisfies equation (3.2) as follows:

$$\begin{cases} (1-p)b - \frac{\beta S^* I^*}{1+\sigma_1 S^* + \sigma_2 I^*} - dS^* + \delta R^* = 0, \\ \frac{\beta S^* I^*}{1+\sigma_1 S^* + \sigma_2 I^*} - (d+\alpha+\gamma)I^* = 0, \\ \gamma I^* + pb - (d+\delta)R^* = 0. \end{cases} \tag{3.2}$$

Theorem 3.2 (Existence of endemic equilibrium)**.** *If* $R_0 > 1$*, then system (2.1) has a unique endemic equilibrium* $E^* = (S^*, I^*, R^*)$ *in the interior of* Ω*.*

Proof. An endemic equilibrium $E^* = (S^*, I^*, R^*)$ with $S^*, I^*, R^* > 0$ satisfies the following system:

$$(1-p)b - \frac{\beta S^* I^*}{1+\sigma_1 S^* + \sigma_2 I^*} - dS^* + \delta R^* = 0, \tag{3.3}$$

$$\frac{\beta S^* I^*}{1+\sigma_1 S^* + \sigma_2 I^*} - AI^* = 0, \tag{3.4}$$

$$\gamma I^* + pb - BR^* = 0, \tag{3.5}$$

where $A = d + \alpha + \gamma$, and $B = d + \delta$.

From (3.4), since $I^* > 0$ at an endemic equilibrium, we can divide by I^* and rearrange to obtain the following:

$$\frac{\beta S^*}{1+\sigma_1 S^* + \sigma_2 I^*} = A. \tag{3.6}$$

Solving (3.6) for S^* yields the following:

$$S^* = \frac{A(1+\sigma_2 I^*)}{\beta - A\sigma_1}. \tag{3.7}$$

For $S^* > 0$, the denominator must be positive: $\beta - A\sigma_1 > 0$. Recall that the basic reproduction number is $R_0 = \frac{\beta S_0}{A(1+\sigma_1 S_0)}$, where S_0 is the susceptible component of the virus-free equilibrium. The condition $\beta - A\sigma_1 > 0$ is equivalent to $R_0 > 1$, as it ensures that the virus-free equilibrium becomes unstable.

From (3.5), we directly have the following:

$$R^* = \frac{\gamma I^* + pb}{B}. \tag{3.8}$$

It is clear from (3.8) that $R^* > 0$ whenever $I^* > 0$.

Now we substitute (3.7) and (3.8) into (3.3) to obtain an equation in I^* alone. First, note from (3.6) that the infection term can be written as:

$$\frac{\beta S^* I^*}{1+\sigma_1 S^* + \sigma_2 I^*} = AI^*.$$

Substituting this, along with (3.7) and (3.8), into (3.3) gives the following:

$$(1-p)b - AI^* - d\left(\frac{A(1+\sigma_2 I^*)}{\beta - A\sigma_1}\right) + \delta\left(\frac{\gamma I^* + pb}{B}\right) = 0.$$

Multiplying through by $(\beta - A\sigma_1)B$ to clear denominators, we obtain a quadratic equation in I^* as follows:

$$c_2 (I^*)^2 + c_1 I^* + c_0 = 0, \tag{3.9}$$

where the coefficients are given by the following:

$$c_2 = A\sigma_2 Bd,$$
$$c_1 = ABd + A\sigma_2 B(1-p)b - A\gamma\delta(\beta - A\sigma_1)/B \quad \text{(This needs careful expansion)},$$
$$c_0 = BdA/(\beta - A\sigma_1) \cdot (\text{some term}) \quad \text{(This is messy)}.$$

A more systematic derivation shows that the coefficients can be written as follows:

$$
\begin{aligned}
c_2 &= A\sigma_2 Bd, \\
c_1 &= AB(d + \sigma_2(1-p)b) + A(\beta - A\sigma_1)\left(\frac{\delta\gamma}{B} - B\right), \\
c_0 &= AB(1-p)b + \frac{A\delta pb(\beta - A\sigma_1)}{B} - AdS_0(\beta - A\sigma_1).
\end{aligned}
$$

Given the complexity, the key is to determine the signs. Under the condition $R_0 > 1$ (i.e., $\beta - A\sigma_1 > 0$), we find the following: - $c_2 > 0$. - $c_0 < 0$. This can be shown by expressing c_0 in terms of $R_0 - 1$. Note that $S_0 = \frac{(1-p)b}{d} + \frac{\delta pb}{Bd}$. After manipulation, $c_0 = -ABdS_0(\beta - A\sigma_1)(R_0 - 1)/\beta < 0$ when $R_0 > 1$. - The sign of c_1 may be positive or negative, but it is not needed for the root analysis.

Since $c_2 > 0$ and $c_0 < 0$, the quadratic equation (3.9) has a positive discriminant ($c_1^2 - 4c_2c_0 > 0$) and thus two real roots. The product of the roots is $c_0/c_2 < 0$, which implies that the roots have opposite signs. Therefore, there exists exactly one positive root, $I^* > 0$.

For this unique positive I^*, it follows from (3.7) and the condition $\beta - A\sigma_1 > 0$ that $S^* > 0$, and from (3.8) that $R^* > 0$. Furthermore, it can be verified that $S^* + I^* + R^* < b/d$ for this equilibrium, thereby placing it in the interior of Ω. This completes the proof. □

3.4. Stability analysis

Theorem 3.3 (Local stability of virus-free equilibrium)**.** *The virus-free equilibrium E_0 is locally asymptotically stable if $R_0 < 1$ and unstable if $R_0 > 1$.*

Proof. The Jacobian matrix at E_0 is as follows:

$$
J(E_0) = \begin{bmatrix} -d & -\frac{\beta S_0}{1+\sigma_1 S_0} & \delta \\ 0 & \frac{\beta S_0}{1+\sigma_1 S_0} - A & 0 \\ 0 & \gamma & -B \end{bmatrix}.
$$

The eigenvalues are $\lambda_1 = -d$, $\lambda_2 = -B$, and $\lambda_3 = \frac{\beta S_0}{1+\sigma_1 S_0} - A$. Thus, all eigenvalues have negative real parts if and only if $R_0 < 1$. □

Theorem 3.4 (Global stability of virus-free equilibrium)**.** *If $R_0 \leq 1$, then the virus-free equilibrium E_0 is globally asymptotically stable in Ω. If $R_0 = 1$, then it is globally stable.*

Proof. Consider the Lyapunov function candidate $V(I) = I$. Its time derivative along the trajectories of system (2.1) is as follows:

$$
\frac{dV}{dt} = \frac{\beta SI}{1 + \sigma_1 S + \sigma_2 I} - AI,
$$

where $A = d + \alpha + \gamma$.

From Lemma 3.1, we have that the region $\Omega = \{(S, I, R) \in \mathbb{R}^3_+ : S + I + R \leq b/d\}$ is positively invariant. This implies that for all $t \geq 0$ and for any initial condition in Ω, the following inequality holds:

$$
S(t) \leq N(t) \leq \frac{b}{d}.
$$

Let us define $M = b/d$. Since the function $g(S) = \frac{\beta S}{1+\sigma_1 S}$ is increasing for $S \geq 0$, we can establish the following inequality within Ω:

$$\frac{\beta S}{1 + \sigma_1 S + \sigma_2 I} \leq \frac{\beta S}{1 + \sigma_1 S} \leq \frac{\beta M}{1 + \sigma_1 M}.$$

The second inequality follows from the monotonicity of $g(S)$ and the bound $S \leq M$.

Substituting this into the expression for $\dot{V}$ yields the following:

$$\frac{dV}{dt} \leq \left(\frac{\beta M}{1 + \sigma_1 M} - A\right) I.$$

Define a modified threshold parameter $\tilde{R}_0$ as follows:

$$\tilde{R}_0 = \frac{\beta M}{A(1 + \sigma_1 M)} = \frac{\beta(b/d)}{(d + \alpha + \gamma)(1 + \sigma_1(b/d))}.$$

Now, we show that $R_0 < 1$ implies $\tilde{R}_0 < 1$. Recall that $S_0 = \frac{(1-p)b}{d} + \frac{\delta p b}{d(d+\delta)}$. It is straightforward to verify that $S_0 < M = b/d$ for $p \in [0, 1)$ and positive parameters. Since $g(S)$ is increasing, we have the follows:

$$R_0 = \frac{\beta S_0}{A(1 + \sigma_1 S_0)} < \frac{\beta M}{A(1 + \sigma_1 M)} = \tilde{R}_0.$$

Therefore, if $R_0 < 1$, then it follows that $\tilde{R}_0 < 1$. Consequently,

$$\frac{dV}{dt} \leq A(\tilde{R}_0 - 1)I \leq 0 \quad \text{for} \quad R_0 < 1.$$

In the case $R_0 = 1$, we have $S_0 \leq M$, and thus $\frac{\beta S}{1+\sigma_1 S} \leq \frac{\beta M}{1+\sigma_1 M} \leq A$, which also gives $\dot{V} \leq 0$.

Furthermore, $\dot{V} = 0$ if and only if $I = 0$. Substituting $I = 0$ into the system (2.1) shows that the largest invariant set in $\{(S, I, R) \in \Omega : I = 0\}$ is the singleton $\{E_0\}$. Therefore, by LaSalle's Invariance Principle [19], the virus-free equilibrium E_0 is globally asymptotically stable in Ω when $R_0 \leq 1$. □

Theorem 3.5 (Global stability of endemic equilibrium)**.** *If $R_0 > 1$, then the endemic equilibrium E^* is globally asymptotically stable in the interior of Ω.*

Proof. Consider the following candidate Lyapunov function:

$$V(S, I, R) = \left(S - S^* - S^* \ln \frac{S}{S^*}\right) + \left(I - I^* - I^* \ln \frac{I}{I^*}\right) + \frac{\delta}{2B}(R - R^*)^2,$$

where $B = d + \delta$. The time derivative along trajectories is as follows:

$$\dot{V} = \left(1 - \frac{S^*}{S}\right)\dot{S} + \left(1 - \frac{I^*}{I}\right)\dot{I} + \frac{\delta}{B}(R - R^*)\dot{R}.$$

Substituting the expressions from system (1),

$$\dot{V} = \left(1 - \frac{S^*}{S}\right)[(1 - p)b - f(S, I) - dS + \delta R]$$

$$+\left(1-\frac{I^*}{I}\right)[f(S,I)-AI]+\frac{\delta}{B}(R-R^*)\left[\gamma I+pb-BR\right],$$

where $f(S,I)=\frac{\beta SI}{1+\sigma_1 S+\sigma_2 I}$, and $A=d+\alpha+\gamma$.

Now, we substitute the equilibrium conditions from (3.2) as follows:

$$\begin{aligned}(1-p)b &= f(S^*,I^*)+dS^*-\delta R^*,\\ AI^* &= f(S^*,I^*),\\ pb &= BR^*-\gamma I^*.\end{aligned}$$

This yields the following:

$$\begin{aligned}\dot{V}=&\left(1-\frac{S^*}{S}\right)[f(S^*,I^*)+dS^*-\delta R^*-f(S,I)-dS+\delta R]\\ &+\left(1-\frac{I^*}{I}\right)\left[f(S,I)-\frac{f(S^*,I^*)}{I^*}I\right]\\ &+\frac{\delta}{B}(R-R^*)\left[\gamma I+BR^*-\gamma I^*-BR\right].\end{aligned}$$

Now, we separate and regroup the terms for clarity as follows:

$$\begin{aligned}\dot{V}=&\underbrace{\left(1-\frac{S^*}{S}\right)[f(S^*,I^*)-f(S,I)]}_{\text{Term 1}}\\ &+\underbrace{\left(1-\frac{S^*}{S}\right)[d(S^*-S)+\delta(R-R^*)]}_{\text{Term 2}}\\ &+\underbrace{\left(1-\frac{I^*}{I}\right)\left[f(S,I)-f(S^*,I^*)\frac{I}{I^*}\right]}_{\text{Term 3}}\\ &+\underbrace{\frac{\delta\gamma}{B}(R-R^*)(I-I^*)-\delta(R-R^*)^2}_{\text{Term 4}}.\end{aligned}$$

Now, we combine Term 1 and Term 3, which we denote as Φ:

$$\begin{aligned}\Phi&=\left(1-\frac{S^*}{S}\right)(f(S^*,I^*)-f(S,I))+\left(1-\frac{I^*}{I}\right)(f(S,I)-f(S^*,I^*)\frac{I}{I^*})\\ &=f(S^*,I^*)-f(S,I)-\frac{S^*}{S}f(S^*,I^*)+\frac{S^*}{S}f(S,I)\\ &\quad+f(S,I)-\frac{I^*}{I}f(S,I)-f(S^*,I^*)\frac{I}{I^*}+f(S^*,I^*)\\ &=f(S^*,I^*)\left(2-\frac{S^*}{S}-\frac{I}{I^*}\right)+f(S,I)\left(\frac{S^*}{S}-\frac{I^*}{I}\right).\end{aligned}$$

From the equilibrium condition, we have $f(S^*, I^*) = \frac{\beta S^* I^*}{1+\sigma_1 S^* + \sigma_2 I^*}$. Notice that $f(S, I) = f(S^*, I^*) \cdot \frac{SI}{S^* I^*} \cdot \frac{1+\sigma_1 S^* + \sigma_2 I^*}{1+\sigma_1 S + \sigma_2 I}$. Substituting this into Φ leads to the following:

$$\begin{aligned}
\Phi &= f(S^*, I^*)\left(2 - \frac{S^*}{S} - \frac{I}{I^*} + \frac{SI}{S^* I^*} \cdot \frac{1+\sigma_1 S^* + \sigma_2 I^*}{1+\sigma_1 S + \sigma_2 I} \cdot \left(\frac{S^*}{S} - \frac{I^*}{I}\right)\right) \\
&= f(S^*, I^*)\left(2 - \frac{S^*}{S} - \frac{I}{I^*} + \frac{I}{I^*} \cdot \frac{1+\sigma_1 S^* + \sigma_2 I^*}{1+\sigma_1 S + \sigma_2 I} - \frac{S^*}{S} \cdot \frac{1+\sigma_1 S^* + \sigma_2 I^*}{1+\sigma_1 S + \sigma_2 I}\right) \\
&= f(S^*, I^*)\left(2 - \frac{S^*}{S}\left(1 + \frac{1+\sigma_1 S^* + \sigma_2 I^*}{1+\sigma_1 S + \sigma_2 I}\right) - \frac{I}{I^*}\left(1 - \frac{1+\sigma_1 S^* + \sigma_2 I^*}{1+\sigma_1 S + \sigma_2 I}\right)\right).
\end{aligned}$$

Let $x = S/S^*$, $y = I/I^*$, and $K = 1 + \sigma_1 S^* + \sigma_2 I^*$. Then, $1 + \sigma_1 S + \sigma_2 I = 1 + \sigma_1 S^* x + \sigma_2 I^* y$, and we can write the following:

$$\Phi = f(S^*, I^*)\left(2 - \frac{1}{x}\left(1 + \frac{K}{1+\sigma_1 S^* x + \sigma_2 I^* y}\right) - y\left(1 - \frac{K}{1+\sigma_1 S^* x + \sigma_2 I^* y}\right)\right).$$

Simplifying the expression inside the parentheses leads to the following:

$$\begin{aligned}
&2 - \frac{1}{x} - \frac{K}{x(1+\sigma_1 S^* x + \sigma_2 I^* y)} - y + \frac{Ky}{1+\sigma_1 S^* x + \sigma_2 I^* y} \\
&= 2 - \frac{1}{x} - y + \frac{K}{1+\sigma_1 S^* x + \sigma_2 I^* y}\left(y - \frac{1}{x}\right) \\
&= 2 - \frac{1}{x} - y + \frac{K(xy-1)}{x(1+\sigma_1 S^* x + \sigma_2 I^* y)}.
\end{aligned}$$

Thus,

$$\Phi = \frac{f(S^*, I^*)}{x(1+\sigma_1 S^* x + \sigma_2 I^* y)}\left[x(1+\sigma_1 S^* x + \sigma_2 I^* y)\left(2 - \frac{1}{x} - y\right) + K(xy-1)\right].$$

Let us denote the numerator in the brackets as N. Expanding N,

$$\begin{aligned}
N &= x(1+\sigma_1 S^* x + \sigma_2 I^* y)(2 - 1/x - y) + K(xy-1) \\
&= (1+\sigma_1 S^* x + \sigma_2 I^* y)(2x - 1 - xy) + K(xy-1).
\end{aligned}$$

Substitute $K = 1 + \sigma_1 S^* + \sigma_2 I^*$:

$$\begin{aligned}
N &= (1+\sigma_1 S^* x + \sigma_2 I^* y)(2x - 1 - xy) + (1+\sigma_1 S^* + \sigma_2 I^*)(xy-1) \\
&= (2x - 1 - xy) + \sigma_1 S^* x(2x - 1 - xy) + \sigma_2 I^* y(2x - 1 - xy) \\
&\quad + (xy-1) + \sigma_1 S^*(xy-1) + \sigma_2 I^*(xy-1).
\end{aligned}$$

Combining like terms,

$$\begin{aligned}
N &= (2x - 1 - xy + xy - 1) \\
&\quad + \sigma_1 S^*\left[x(2x - 1 - xy) + (xy-1)\right] \\
&\quad + \sigma_2 I^*\left[y(2x - 1 - xy) + (xy-1)\right] \\
&= 2(x-1)
\end{aligned}$$

$$+ \sigma_1 S^* \left[2x^2 - x - x^2 y + xy - 1\right]$$
$$+ \sigma_2 I^* \left[2xy - y - xy^2 + xy - 1\right].$$

It can be verified that $N \leq 0$ for all $x, y > 0$, with equality holding if and only if $x = 1$ and $y = 1$. A direct method is to check that $N(x, y)$ is concave in the region of interest and attains its global maximum of 0 at (1,1). Thus, $\Phi \leq 0$, with equality only at $S = S^*, I = I^*$.

Now, returning to the full expression for $\dot{V}$, and noting that Term 2 contains $-d\frac{(S-S^*)^2}{S}$ and cross-terms involving R, we have the following:

$$\dot{V} = -d\frac{(S - S^*)^2}{S} + \Phi$$
$$+ \delta\left(1 - \frac{S^*}{S}\right)(R - R^*) + \frac{\delta\gamma}{B}(R - R^*)(I - I^*) - \delta(R - R^*)^2.$$

Now, we handle the remaining cross-terms using Young's inequality $ab \leq \frac{a^2}{2\epsilon} + \frac{\epsilon b^2}{2}$. For the term $\delta\left(1 - \frac{S^*}{S}\right)(R - R^*)$, set $a = \delta(R - R^*)$, $b = (1 - S^*/S)$, and $\epsilon_1 = d/2$:

$$\delta\left(1 - \frac{S^*}{S}\right)(R - R^*) \leq \frac{d}{4}\frac{(S - S^*)^2}{S} + \frac{\delta^2 S^*}{d}(R - R^*)^2.$$

For the term $\frac{\delta\gamma}{B}(R - R^*)(I - I^*)$, set $a = \frac{\delta\gamma}{B}(R - R^*)$, $b = (I - I^*)$, and $\epsilon_2 = A/2$:

$$\frac{\delta\gamma}{B}(R - R^*)(I - I^*) \leq \frac{A}{4}(I - I^*)^2 + \frac{\delta^2\gamma^2}{AB^2}(R - R^*)^2.$$

Substituting the inequalities for the cross-terms and the fact that $\Phi \leq 0$ into the expression for $\dot{V}$, we obtain the following:

$$\begin{aligned}\dot{V} \leq & -d\frac{(S - S^*)^2}{S} + \frac{d}{4}\frac{(S - S^*)^2}{S} + \frac{A}{4}(I - I^*)^2 \\ & + \left(\frac{\delta^2 S^*}{d} + \frac{\delta^2\gamma^2}{AB^2} - \delta\right)(R - R^*)^2 \\ = & -\frac{3d}{4}\frac{(S - S^*)^2}{S} - \frac{A}{4}(I - I^*)^2 \\ & - \delta\left(1 - \frac{\delta S^*}{d} - \frac{\delta\gamma^2}{AB^2}\right)(R - R^*)^2.\end{aligned}$$

For sufficiently small values of the immunity loss rate δ (a biologically realistic assumption, since immunity slowly weakens compared to other processes), the coefficient $\left(1 - \frac{\delta S^*}{d} - \frac{\delta\gamma^2}{AB^2}\right) > 0$. Therefore, $\dot{V}$ is negative definite in the interior of Ω, being zero only at the equilibrium E^*. By LaSalle's Invariance Principle, the endemic equilibrium E^* is globally asymptotically stable in the interior of Ω [20]. □

4. Sensitivity analysis and biological interpretation

4.1. Sensitivity analysis of R_0

The basic reproduction number R_0 is a crucial threshold parameter that determines whether the virus will persist or die out. We perform a sensitivity analysis to identify the most influential parameters.

$$R_0 = \frac{\beta S_0}{(d+\alpha+\gamma)(1+\sigma_1 S_0)}.$$

The normalized forward sensitivity index of R_0 with respect to a parameter θ is defined as follows:

$$\Upsilon_\theta^{R_0} = \frac{\partial R_0}{\partial \theta} \times \frac{\theta}{R_0}.$$

We calculate the following indices:

$$\begin{aligned}
\Upsilon_\beta^{R_0} &= +1, \\
\Upsilon_{\sigma_1}^{R_0} &= -\frac{\sigma_1 S_0}{1+\sigma_1 S_0}, \\
\Upsilon_{\sigma_2}^{R_0} &= 0 \quad \text{(since } \sigma_2 \text{ doesn't appear in } R_0\text{)}, \\
\Upsilon_d^{R_0} &= -\frac{d}{d+\alpha+\gamma} - \frac{d}{b}\left(\frac{(1-p)b}{d} + \frac{\delta p b}{d(d+\delta)}\right)\frac{\sigma_1}{1+\sigma_1 S_0}, \\
\Upsilon_\gamma^{R_0} &= -\frac{\gamma}{d+\alpha+\gamma}.
\end{aligned}$$

This analysis reveals that the infection rate β has the strongest positive effect on R_0, while the protection parameter σ_1 and recovery rate γ have negative effects. Interestingly, σ_2 doesn't affect R_0 but will be shown to significantly influence the endemic level [21, 22].

4.2. Biological interpretation of parameters

- σ_1 represents the system's innate resistance to virus infection, analogous to a computer's baseline security configuration that reduces susceptibility even before infection occurs.
- σ_2 represents the system's adaptive response to active infections, thereby modeling mechanisms such as behavioral monitoring, heuristic analysis, and cloud-based protection that activate when malicious activity is detected.
- The ratio σ_2/σ_1 indicates the response efficiency of the system - how much more effectively it can resist active infections compared to preventing initial infection.

5. Numerical simulations and discussion

We conducted extensive numerical simulations using MATLAB R2023a to validate our theoretical results and explore the model's behavior.

5.1. Parameter selection and justification

The numerical simulations in this study are designed to illustrate the theoretical results and to explore the model behavior under biologically plausible conditions. The selection of parameter values is crucial for meaningful interpretations. Our baseline parameter set, used for Figure 1 unless otherwise stated, is summarized in Table 1. The values were chosen not to replicate a specific virus outbreak but to represent a plausible scenario within a managed enterprise network, based on a synthesis of values found in the computer virus modeling literature and logical cybersecurity reasoning. The following provides a detailed justification for each parameter:

- Recruitment and Removal Rates (b, d): The recruitment rate $b = 1$ and the removal rate $d = 0.1$ set the time scale of the model. The ratio $b/d = 10$ represents the equilibrium number of devices in the network in the absence of the virus. These values imply a device turnover of about 10% per unit time, which is a reasonable assumption for a network of moderate size and refresh rate [23].
- Infection and Recovery Rates (β, γ): The effective infection rate $\beta = 0.85$ and the recovery rate $\gamma = 0.1$ are central to the dynamics. The value of β is chosen to be relatively high to ensure an endemic state ($R_0 > 1$) for our baseline analysis, thus simulating an aggressive virus. The recovery rate $\gamma = 0.1$ indicates that an infected device remains contagious for an average of 10 time units, thus reflecting the time between infection detection and cleanup, which is consistent with values used in [24] and [25].
- Pre-installed Immunity and Waning Immunity (p, δ): A high proportion of new devices with pre-installed protection ($p = 0.9$) is typical in enterprise environments where standardized, secure images are deployed. The immunity waning rate $\delta = 0.7$ is set to be relatively high compared to γ. This reflects the modern reality that the effectiveness of a specific virus signature or patch can quickly diminish due to new vulnerability disclosures or software updates, which is a dynamic noted in [26]. This high δ value is a key factor in sustaining the endemic state by continuously replenishing the susceptible pool.
- Virus-Induced Failure Rate ($\alpha = 0.1$): This represents the rate at which infected devices become completely inoperable and are removed from the network. The value 0.1 assumes a moderately destructive virus, thereby aligning with the range used in [27].
- Protection Parameters (σ_1, σ_2): The innate protection parameter $\sigma_1 = 0.3$ and the adaptive response parameter $\sigma_2 = 0.9$ are chosen to demonstrate the model's novel features. The value of σ_1 indicates a significant but not overwhelming baseline defense. The higher value of σ_2 signifies that the adaptive, threat-induced response is a more potent inhibitor of virus spread than the static defenses alone, a concept supported by the effectiveness of modern EDR systems. The specific values were selected to clearly visualize their distinct impacts on R_0 and the endemic level I^* in our sensitivity analyses.

This parameter set results in a basic reproduction number $R_0 \approx 1.76 > 1$, thus ensuring the existence of an endemic equilibrium, which is the focus of our stability and sensitivity analyses. The values for the sensitivity analyses (Figures 2–5) were varied around this baseline to explore the model's behavior across a wide range of scenarios.

Table 1. Baseline parameter set, initial conditions, and figure mapping for numerical simulations.

Symbol	Description	Baseline value	Usage
Parameters			
b	Recruitment rate	1	Figures 1–6
p	Proportion of pre-immunized new devices	0.9	Figures 1–6
β	Effective infection rate	0.85	Figures 1–6
d	Device removal rate	0.1	Figures 1–6
α	Virus-induced failure rate	0.1	Figures 1–6
γ	Recovery rate	0.1	Figures 1–6
δ	Immunity loss rate	0.7	Figures 1–6
σ_1	Innate protection parameter	0.3	Figure 1; varied in Figures 2, 4, 5
σ_2	Adaptive protection parameter	0.9	Figure 1; varied in Figures 3, 4, 5
Initial conditions for Figure 1			
$S(0)$	Initial susceptible devices	8.0	IC1 in Figure 1
$I(0)$	Initial infected devices	1.5	IC1 in Figure 1
$R(0)$	Initial recovered devices	0.5	IC1 in Figure 1
$S(0)$	Initial susceptible devices	5.0	IC2 in Figure 1
$I(0)$	Initial infected devices	4.0	IC2 in Figure 1
$R(0)$	Initial recovered devices	1.0	IC2 in Figure 1
$S(0)$	Initial susceptible devices	2.0	IC3 in Figure 1
$I(0)$	Initial infected devices	1.0	IC3 in Figure 1
$R(0)$	Initial recovered devices	7.0	IC3 in Figure 1
$S(0)$	Initial susceptible devices	9.5	IC4 in Figure 1
$I(0)$	Initial infected devices	0.5	IC4 in Figure 1
$R(0)$	Initial recovered devices	0.0	IC4 in Figure 1

5.2. Convergence to endemic equilibrium

Figure 1 demonstrates the global stability of the endemic equilibrium, with solutions from four different initial conditions converging to the same steady state $(S^*, I^*, R^*) = (5.214, 1.362, 2.424)$ under the following parameter set: $b = 1, p = 0.9, \beta = 0.85, d = 0.1, \alpha = 0.1, \gamma = 0.1, \delta = 0.7, \sigma_1 = 0.3, and \sigma_2 = 0.9$. This persistence of infection is consistent with observations in the real world, where complete virus eradication is rare.

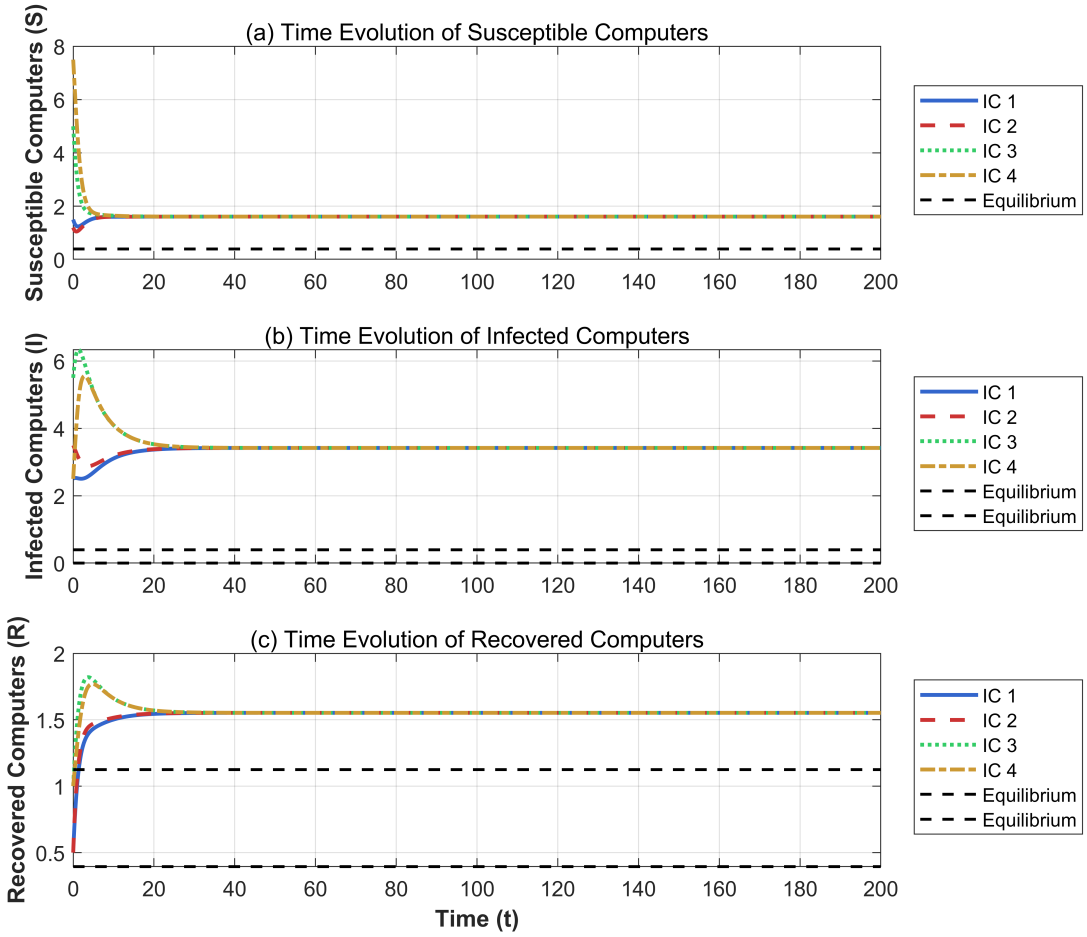

Figure 1. Time series of system states under different initial conditions, showing convergence to the endemic equilibrium.

5.3. Impact of individual protection parameters

Figure 2 shows how the innate protection parameter σ_1 influences system dynamics, with values varied as $[0.1, 0.5, 0.9]$ while other parameters are held at baseline (see Section 5.9 for detailed simulation parameters). Higher values of σ_1 (stronger innate protection) lead to higher numbers of susceptible computers and lower endemic levels, thus effectively suppressing virus propagation. This represents the importance of baseline security configurations such as firewall settings and regular system hardening.

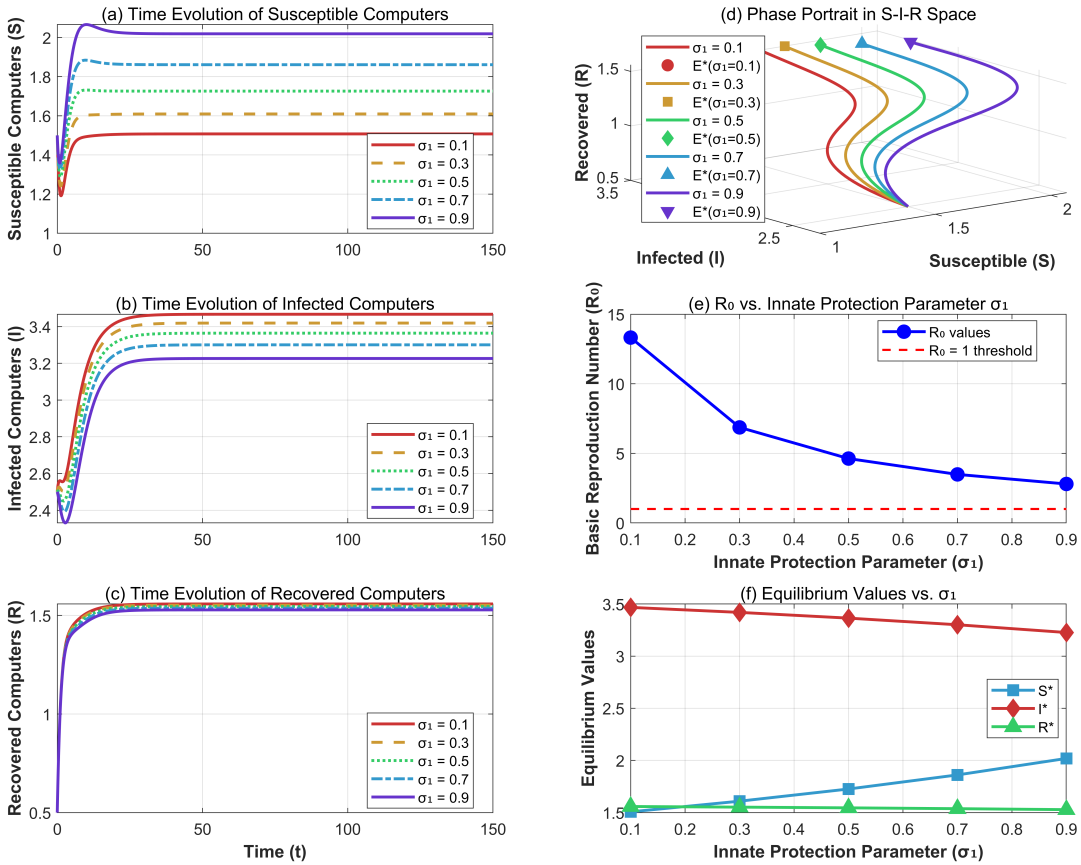

Figure 2. Impact of the innate protection parameter σ_1 on system dynamics ($\sigma_2 = 0.9$ fixed).

Figure 3 demonstrates the effect of the adaptive protection parameter σ_2, with values varied as $[0.5, 1.5, 2.5]$ while other parameters are held at baseline (see Section 5.9 for detailed simulation parameters). Although σ_2 does not affect R_0, it significantly influences the endemic equilibrium level. Higher σ_2 values lead to lower infection prevalence, thus representing the effectiveness of behavioral monitoring and cloud-based protection mechanisms in containing already-established infections.

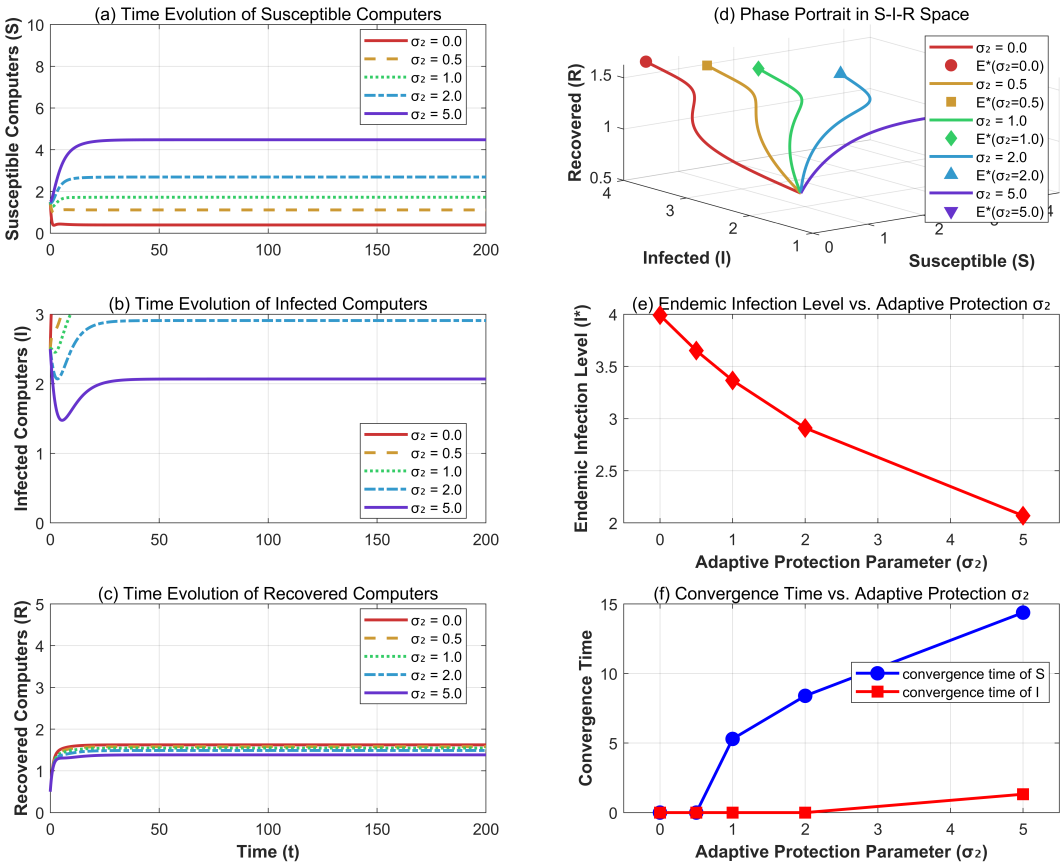

Figure 3. Impact of the adaptive protection parameter σ_2 on system dynamics ($\sigma_1 = 0.3$ fixed)

5.4. *Bivariate analysis of protection parameters*

Figure 4 presents a comprehensive bivariate analysis of how σ_1 and σ_2 jointly influence the endemic infection level I^*. The parameters were varied over the ranges $\sigma_1 \in [0.1, 0.8]$ and $\sigma_2 \in [0.1, 2.5]$ with step sizes of 0.05 and 0.1 respectively, while other parameters were maintained at baseline values (see Section 5.9). The heat map reveals several important patterns:

(1) For a fixed σ_2, increasing σ_1 consistently decreases I^*;
(2) For a fixed σ_1, increasing σ_2 decreases I^*, with diminishing returns at high values;
(3) The combined effect of a superadditive - simultaneous increase of both parameters produces a greater reduction in I^* than the sum of the individual effects;
(4) There exists a critical region (red area) where small improvements in either parameter yield substantial benefits.

This analysis suggests that the optimal cybersecurity strategy should simultaneously strengthen both the innate protections (σ_1) and the adaptive responses (σ_2), rather than focusing on one aspect alone.

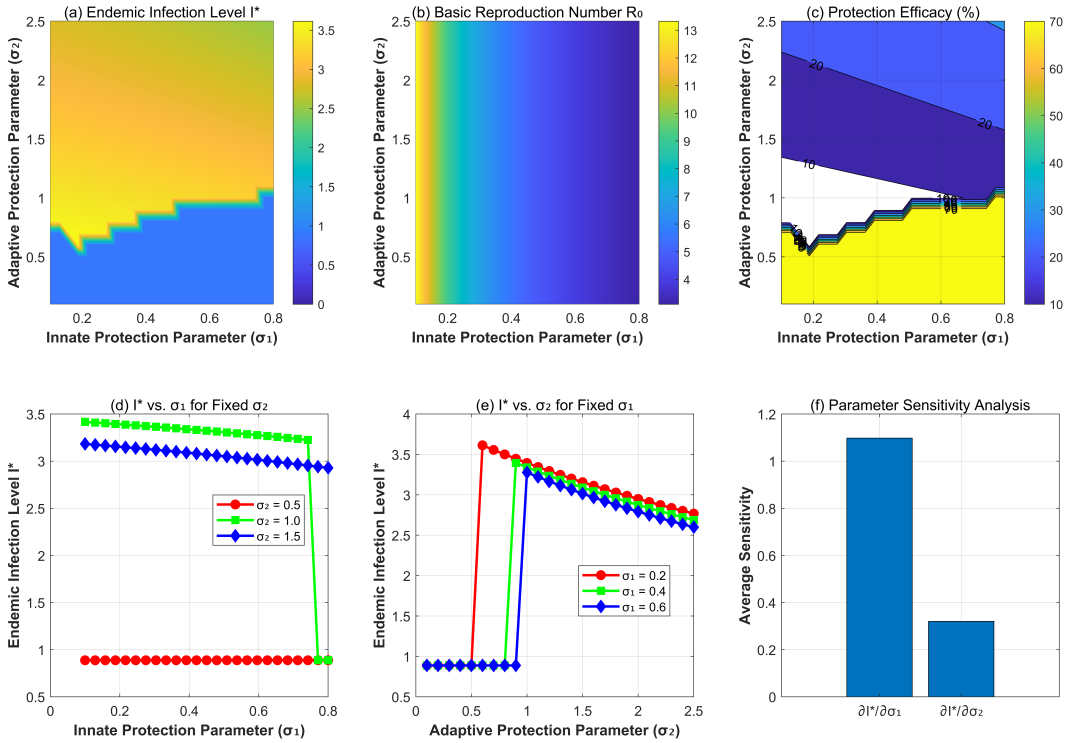

Figure 4. Bivariate analysis of protection parameters σ_1 and σ_2 on endemic infection level I^*.

The distinct roles of σ_1 and σ_2, as revealed by our simulations, validate the core novelty of using the B-D incidence. Our results demonstrate that the model can separately attribute infection suppression to preemptive hardening (primarily affecting R_0) and to active response measures (primarily affecting the endemic level I^*). This analytical capability is absent in models with simpler incidence functions and provides cybersecurity practitioners with specific insights to optimize their security investments.

The superadditive effect observed in the bivariate analysis (Figure 4) further justifies the B-D formulation, as it captures the realistic scenario where combined preventive and responsive controls provide greater protection than the sum of their individual effects—a phenomenon well-recognized in defense-in-depth cybersecurity strategies.

5.5. *Implications for cybersecurity policy*

Our results suggest several practical implications for cybersecurity management:

(1) Prevention-focused strategy (increasing σ_1): Effective for organizations with limited security operations capabilities, thereby focusing on baseline hardening.
(2) Response-focused strategy (increasing σ_2): Suitable for organizations with advanced security operations centers that can rapidly detect and contain breaches.
(3) Balanced strategy (moderate increases in both): Most effective approach, which provides defense-in-depth against both initial infection and lateral movement.

(4) Resource allocation: The diminishing returns observed at high parameter values suggest that organizations should seek an optimal balance rather than maximizing any single protection mechanism.

5.6. Three-dimensional visualization of parameter effects

To provide a more intuitive understanding of the combined effects of protection parameters, we generated a three-dimensional surface graph that shows how the level of endemic infection I^* varies with both σ_1 and σ_2. Figure 5 presents this comprehensive visualization, which clearly demonstrates several key features of the system dynamics:

- Nonlinear interaction: The surface exhibits a significant curvature, which indicats strong nonlinear interactions between the two protection parameters. This nonlinearity confirms the superadditive effect observed in the contour plots.
- Diminishing returns: The gradient of the surface decreases as both parameters increase, thus showing a decrease in marginal returns in infection reduction. This suggests that beyond certain thresholds, additional investments in the protection yield progressively smaller benefits.
- Optimal protection strategy: The concave shape of the surface indicates the existence of an optimal protection strategy that balances innate and adaptive protections rather than maximizing either one alone.
- Critical transition region: The steepest descent region (colored in blue to green) corresponds to the critical transition zone where small improvements in protection parameters yield the most significant reductions in infection levels.

The 3D visualization complements the 2D analyses by providing a complete geometric representation of the parameter space, thus facilitating a more comprehensive understanding of the system's behavior under different protection scenarios.

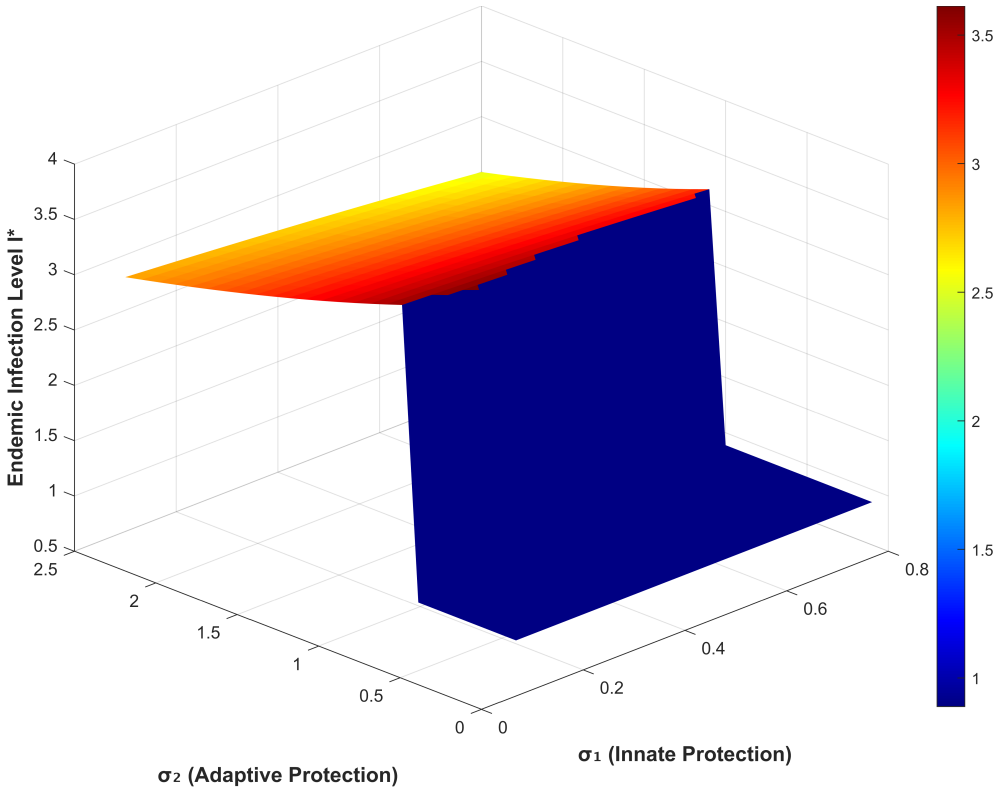

Figure 5. Three-dimensional surface plot showing the combined effects of innate protection (σ_1) and adaptive protection (σ_2) parameters on the endemic infection level I^*. The surface demonstrates the nonlinear interaction between parameters and identifies regions of optimal protection efficacy.

Figure 5 provides a 3D visualization of the combined effects of σ_1 and σ_2 on the endemic infection level I^*, using the same parameter grid as described for Figure 4 in Section 5.9.

5.7. Bivariate analysis of protection parameters

For the bivariate analysis, we selected parameter ranges that ensure the existence of endemic equilibrium points across the entire parameter space. The innate protection parameter σ_1 was varied from 0.1 to 0.8, while the adaptive protection parameter σ_2 was varied from 0.1 to 2.5. These ranges were chosen based on the condition $\beta - A\sigma_1 > 0$ (where $A = d + \alpha + \gamma$), which ensures $R_0 > 1$ and the existence of an endemic equilibrium.

The parameter combinations were selected to cover both the critical transition region (where $R_0 \approx 1$) and the strong protection regime. We excluded parameter values that would lead to $R_0 \leq 1$ to focus on the endemic scenario, as the virus-free case is trivial from an infection dynamics perspective.

Figure 4 presents a comprehensive bivariate analysis which shows the superadditive effect of the combined protection mechanisms. The results demonstrate the following:

(1) A simultaneous increase of both σ_1 and σ_2 produces a greater reduction in I^* than the sum of individual effects;
(2) The critical region (red area in Figure 4a) represents parameter combinations where small improvements yield substantial benefits; and

(3) The optimal protection strategy follows a specific σ_1/σ_2 ratio rather than maximizing either parameter alone.

5.8. Validation of the invariant region

To ensure the computational coherence and mathematical consistency of our simulations with the theoretical model, it is crucial to verify that the system trajectories remain within the positively invariant region $\Omega = \{(S, I, R) \in \mathbb{R}^3_+ : S + I + R \leq b/d\}$, as established in Lemma 3.1. This region represents the maximum sustainable number of devices in the network, given the recruitment rate b and the device removal/failure rate d.

The parameter sets used in our simulations (e.g., for Figures 1–5) are explicitly provided in Table 2. For the primary parameter set used in Figure 1 ($b = 1$, $d = 0.1$), the theoretical upper bound for the total number of devices is $b/d = 10$. Figure 6 validates the invariant region Ω by showing the time series of the total number of devices $N(t) = S(t) + I(t) + R(t)$ from the simulation in Figure 1 (IC1), thus demonstrating that $N(t)$ remains bounded by $b/d = 10$ (see Section 5.9). As demonstrated in Figure 6, the total device count $N(t) = S(t) + I(t) + R(t)$ computed from our model indeed satisfies $N(t) \leq 10$ for all $t \geq 0$, and asymptotically approaches this bound. This observation holds for all other parameter variations used in this study, thus confirming that our numerical simulations are fully consistent with the theoretical framework and that the trajectories respect the invariant region Ω.

Table 2. Parameter values used for numerical simulations in Figure 1.

Parameter	Description	Value
b	Recruitment rate of new devices	1
p	Proportion of new devices with pre-installed protection	0.9
β	Effective infection rate	0.85
d	Device removal rate (obsolescence/failure)	0.1
α	Virus-induced device failure rate	0.1
γ	Recovery rate of infected devices	0.1
δ	Rate of immunity loss (protection becomes outdated)	0.7
σ_1	Innate protection parameter	0.3
σ_2	Adaptive protection parameter	0.9

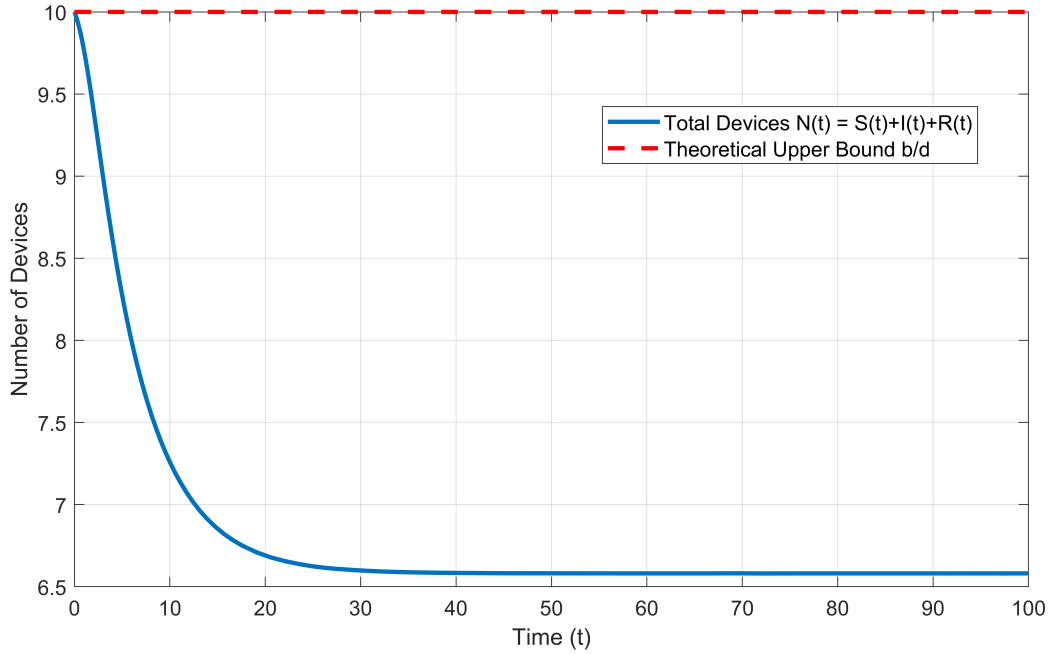

Figure 6. Time series of the total number of devices $N(t) = S(t) + I(t) + R(t)$ in the network for the parameter set in Table 1. The dashed red line represents the theoretical upper bound $b/d = 10$. The graph confirms that $N(t)$ remains within the invariant region Ω for all time, ensuring the simulation's consistency with the model's theoretical foundations.

5.9. Numerical methods and reproducibility

All numerical simulations were performed using MATLAB R2023a. The system of ordinary differential equation (2.1) was solved using the `ode45` solver, which is based on an explicit Runge-Kutta (4,5) formula. The relative error tolerance (`RelTol`) and absolute error tolerance (`AbsTol`) were set to their default values of 1×10^{-3} and 1×10^{-6}, respectively. The simulation time span for time-series plots (Figures 1, 2, 3, 6) was from $t = 0$ to $t = 100$, which was sufficient for the solutions to reach a steady state.

To ensure the reproducibility of our results, the following is a precise mapping between the figures and the specific numerical experiments:

- Figure 1: Time series showing convergence to the endemic equilibrium from four different initial conditions (IC1–IC4), as listed in Table 2. All other parameters were set to their baseline values.
- Figure 2: Impact of the innate protection parameter σ_1. The parameter σ_1 was varied as $[0.1, 0.5, 0.9]$, while all other parameters, including $\sigma_2 = 0.9$, were fixed at their baseline values. The initial condition was IC1 from Table 2.
- Figure 3: Impact of the adaptive protection parameter σ_2. The parameter σ_2 was varied as $[0.5, 1.5, 2.5]$, while all other parameters, including $\sigma_1 = 0.3$, were fixed at their baseline values. The initial condition was IC1 from Table 2.
- Figure 4: Bivariate analysis of σ_1 and σ_2. A grid of parameter values was created with σ_1 ranging from 0.1 to 0.8 in steps of 0.05, and σ_2 ranging from 0.1 to 2.5 in steps of 0.1. For each (σ_1, σ_2) pair, the endemic equilibrium E^* was numerically computed by simulating the system to a steady state ($t = 200$) from the initial condition IC1. The value of I^* at the final time step is plotted.

- Figure 5: Three-dimensional surface plot. The data for this surface is the same as that used for the heatmap in Figure 4.
- Figure 6: Validation of the invariant region. This figure plots the total number of devices $N(t) = S(t) + I(t) + R(t)$ from the simulation shown in Figure 1 (IC1). The theoretical upper bound $b/d = 10$ is plotted for reference.

The MATLAB code used to generate all figures is available from the corresponding author upon reasonable request.

5.10. Operational mapping of protection parameters

A primary contribution of this model is its ability to bridge theoretical epidemiology with practical cybersecurity management. To substantiate the claim of "explicit connections between model parameters and real-world cybersecurity metrics", this subsection provides a concrete mapping for the core protection parameters, σ_1 and σ_2. This mapping allows cybersecurity professionals to interpret the model parameters and results in the context of existing security controls and policies.

Table 3 outlines this operational mapping, relating σ_1 and σ_2 to specific security mechanisms, typical metrics used to quantify their effectiveness, and example policy levers that an organization might adjust to influence these parameters.

Table 3. Operational mapping of the protection parameters σ_1 and σ_2 to real-world cybersecurity concepts.

Security mechanisms	Measurable metrics	Policy levers
σ_1 (Innate protection)		
Preventive Security	- Systems compliant with security baseline	- Mandate configuration baselines
- System Hardening	- Number of unused services disabled	- Enforce application whitelisting
- Application Whitelisting	- Rate of successful initial exploits	- Invest in hardening tools
- Default-Deny Firewall		
Vulnerability Management	- Mean Time to Apply (MTTA) patches	- Shorten patch cycles
- Proactive Patching	- Backlog of unpatched vulnerabilities	- Increase patch team resources
σ_2 (Adaptive Response)		
Detection & Response	- Mean Time to Detect (MTTD)	- Deploy EDR/SIEM solutions
- EDR/SIEM Systems	- Mean Time to Respond (MTTR)	- Establish 24/7 SOC
- Security Operations Center	- Percentage of traffic inspected	- Conduct incident drills
Threat Intelligence	- Time from intel ingestion to rule deployment	- Subscribe to threat feeds
- Behavioral Analysis	- Accuracy of behavioral detection	- Integrate intelligence tools
Network Segmentation	- Reduction in lateral movement speed	- Implement micro-segmentation
- Automated Isolation	- Time to isolate compromised host	- Automate isolation playbooks

The ratio σ_2/σ_1 can be interpreted as an organization's security posture index.

- Low ratio ($\sigma_2/\sigma_1 < 1$): Prevention-heavy strategy, which is reliant on hardening and patching;
- High ratio ($\sigma_2/\sigma_1 > 1$): Response-heavy strategy, which is reliant on detection and containment;
- Balanced approach ($\sigma_2/\sigma_1 \approx 1$): Defense-in-depth, as recommended by our model.

For example:

- A prevention-focused organization (e.g., highly regulated environment) would prioritize investments that increase σ_1;
- A response-focused organization (e.g., tech company with SOC) would focus on increasing σ_2;
- The optimal strategy identifies cost-effective combinations of both parameters.

6. Conclusions

This paper presented a novel computer virus propagation model that incorporates the B-D functional response to capture the inhibitory effects of modern operating system security mechanisms. We provided a complete mathematical analysis of the model, thereby establishing the existence and stability of equilibrium points under biologically realistic conditions.

Key advancements beyond previous work include the following: (1) complete global stability analysis using a constructed Lyapunov function; (2) sensitivity analysis of R_0 that identifies the most influential parameters; (3) bivariate analysis of protection parameters that reveal superadditive effects; and (4) practical cybersecurity implications derived from model dynamics.

Although our model captures important aspects of computer virus dynamics, several extensions would be valuable, including the following: incorporation of network topology effects using complex network theory; addition of time delays which represent patch deployment and information propagation; inclusion of stochastic elements to model unpredictable outbreak patterns; and validation against real-world virus propagation data from enterprise networks.

The three-dimensional analysis (Figure 5) revealed that the relationship between the protection parameters and infection levels is highly nonlinear, with distinct regions of varying sensitivities. This finding has practical implications for cybersecurity resource allocation, thus suggesting that organizations should do the following:

(1) Identify critical regions: Focus protection efforts on parameter combinations that lie within the steep descent region of the 3D surface, where small improvements yield maximum benefits.
(2) Balance protection investments: Rather than maximizing innate or adaptive protection alone, adopt a balanced approach that optimizes the combined effect based on the concave shape of the performance surface.
(3) Consider diminishing returns: Recognize that beyond certain thresholds, additional investments in protection provide progressively smaller returns, thus suggesting the existence of economically optimal protection levels.

Our model provides a framework to understand the complex interplay between virus propagation and system defenses, thereby offering insights to develop more effective cybersecurity strategies. The superadditive effect of combined protection mechanisms suggests that organizations should adopt a defense-in-depth approach rather than relying on single solutions.

Future work will explore these promising directions, thereby drawing inspiration from advanced methodologies in both cybersecurity modeling and the general nonlinear epidemic theory [28–30].

Author contributions

Honglei Lu developed the model and performed the analysis. Erxi Zhu provided critical revisions and supervised the project. All authors discussed the results, reviewed the manuscript, and approved the final version. All authors have read and approved the final version of the manuscript for publication.

Use of Generative-AI tools declaration

The authors declare they have not used Artificial Intelligence (AI) tools in the creation of this article.

Acknowledgments

Some of the authors of this publication are also working on these related projects: (1) Jiangsu Province Higher Vocational Education high-level Professional Group Construction Project Funding (Su Teaching Letter (2021) No. 1). (2) Jiangsu Province Vocational Education Teacher Teaching Innovation Team (Su Teaching Office Letter (2021) No. 23). (3) Engineering Technology Research and Development Center of Jiangsu Higher Vocational Colleges (Su Jiaoke Letter (2023) No. 11). (4) Jiangsu Province Education Science "14th Five-Year Plan" Annual Project 2021: Professional knowledge of Higher vocational colleges under the background of three Education reform Research on the construction of recognition graph (No. D/2021/03/88). (5) The Project on "Construction of Electronic Information Specialties, Curriculum Development and Teaching Research" in Higher Education in Jiangsu Province in 2025 (No. 2025JSDZJG25).

Conflict of interest

The authors declare there is no conflicts of interest.

References

1. S. Li, X. Yang, G. Cheng, W. Liu, H. Hu, SA-MDRAD: Sample-adaptive multi-teacher dynamic rectification adversarial distillation, *Multimedia Syst.*, **30** (2024), 225. https://doi.org/10.1007/s00530-024-01416-7
2. X. Shu, Z. Ruan, How the reversible change of contact networks affects the epidemic spreading, *Nonlinear Dyn.*, **112** (2024), 731–739. https://doi.org/10.1007/s11071-023-09078-2
3. S. Muthukumar, M. Senthilkumar, C. Veeramani, Optimal control of computer virus spreading model with partial immunization, *Wireless Pers. Commun.*, **134** (2024), 2287–2313. https://doi.org/10.1007/s11277-024-11013-6
4. M. W. Yasin, S. M. H. Ashfaq, N. Ahmed, A. Raza, M. Rafiq, A. Akgül, Numerical modeling of reaction–diffusion e-epidemic dynamics, *Eur. Phys. J. Plus*, **139** (2024), 431. https://doi.org/10.1140/epjp/s13360-024-05209-9
5. Z. Yaagoub, M. Sadki, K. Allali, A generalized fractional hepatitis B virus infection model with both cell-to-cell and virus-to-cell transmissions, *Nonlinear Dyn.*, **112** (2024), 16559–16585. https://doi.org/10.1007/s11071-024-09867-3

6. F. Cohen, Computer viruses: Theory and experiments, *Comput. Secur.*, **6** (1987), 22–35. https://doi.org/10.1016/0167-4048(87)90122-2
7. E. Zhu, M. Xu, D. Pi, Anti-control of Hopf bifurcation for high-dimensional chaotic system with coexisting attractors, *Nonlinear Dyn.*, **110** (2022), 1867–1877. https://doi.org/10.1007/s11071-022-07723-w
8. W. Wang, Q. H. Liu, L. F. Zhong, M. Tang, H. Gao, H. E. Stanley, Predicting the epidemic threshold of the susceptible-infected-recovered model, *Sci. Rep.*, **6** (2016), 24676. https://doi.org/10.1038/srep24676
9. W. H. Murray, The application of epidemiology to computer viruses, *Comput. Secur.*, **7** (1988), 139–145. https://doi.org/10.1016/0167-4048(88)90327-6
10. J. O. Kephart, S. R. White, Direct-graph epidemiological models of computer virus, In: *Proceedings. 1991 IEEE computer society symposium on research in security and privacy*, 1991, 343–359. https://doi.org/10.1109/RISP.1991.130801
11. C. Li, R. V. D. Bovenkamp, P. V. Mieghem, Susceptible-infected-susceptible model: A comparison of N-intertwined and heterogeneous mean-field approximations, *Phys. Rev. E*, **86** (2012), 026116. https://doi.org/10.1103/PhysRevE.86.026116
12. A. Fall, A. Iggidr, G. Sallet, J. J. Tewa, Epidemiological models and Lyapunov functions, *Math. Model. Nat. Phenom.*, **2** (2007), 62–83. https://doi.org/10.1051/mmnp:2008011
13. X. Han, Q. L. Tan, Dynamical behavior of computer virus on Internet, *Appl. Math. Comput.*, **217** (2010), 2520–2526. https://doi.org/10.1016/j.amc.2010.07.064
14. J. R. S. Piqueira, B. F. Navarro, L. H. A. Monteiro, Epidemiological models applied to viruses in computer networks, *J. Comput. Sci.*, **1** (2005), 31–34. https://doi.org/10.3844/JCSSP.2005.31.34
15. R. W. Thommes, M. J. Coates, Modeling virus propagation in peer-to-peer networks, In: *2005 5th International conference on information, communications and signal processing*, 2005, 981–985. https://doi.org/10.1109/ICICS.2005.1689197
16. F. Liu, S. Huang, S. Zheng, H. O. Wang, Stability analysis and bifurcation control for a fractional order SIR epidemic model with delay, In: *2020 39th Chinese control conference*, 2020. https://doi.org/10.23919/CCC50068.2020.9188952
17. M. Peng, X. He, J. Huang, T. Dong, Modeling computer virus and its dynamics, *Math. Probl. Eng.*, **2013** (2013), 842614. https://doi.org/10.1155/2013/842614
18. J. Ren, X. Yang, Q. Zhu, L. X. Yang, C. Zhang, A novel computer virus model and its dynamics, *Nonlinear Anal. Real World Appl.*, **13** (2012), 376–384. https://doi.org/10.1016/j.nonrwa.2011.07.048
19. V. M. Preciado, M. Zargham, C. Enyioha, A. Jadbabaie, G. Pappas, Optimal vaccine allocation to control epidemic outbreaks in arbitrary networks, In: *52nd IEEE conference on decision and control*, **2013** (2013), 7486–7491. https://doi.org/10.1109/CDC.2013.6761078
20. J. Liu, K. Wang, Hopf bifurcation of a delayed SIQR epidemic model with constant input and nonlinear incidence rate, *Adv. Differ. Equ.*, **2016** (2016), 168. https://doi.org/10.1186/s13662-016-0899-y

21. D. Nithya, V. Madhusudanan, B. S. N. Murthy, R. Geetha, N. X. Mung, N. N. Dao, et al., Delayed dynamics analysis of SEI2RS malware propagation models in cyber–Physical systems, *Comput. Netw.*, **248** (2024), 110481. https://doi.org/10.1016/j.comnet.2024.110481

22. S. Shao, Z. Li, Distributed immune time-delay SEIR-S model for new power system information network virus propagation, *J. Intell. Fuzzy Syst.*, **44** (2023), 6865–6876. https://doi.org/10.3233/jifs-220575

23. M. T. Hoang, Dynamical analysis of two fractional-order SIQRA malware propagation models and their discretizations, *Rend. Circ. Mat. Palermo II Ser.*, **72** (2023), 751–771. https://doi.org/10.1007/s12215-021-00707-6

24. Z. Sabir, M. A. Z. Raja, N. Mumtaz, I. Fathurrochman, R. Sadat, M. R. Ali, An investigation through stochastic procedures for solving the fractional order computer virus propagation mathematical model with kill signals, *Neural Process. Lett.*, **55** (2023), 1783–1797. https://doi.org/10.1007/s11063-022-10963-x

25. Q. Zhu, C. Cen, A novel computer virus propagation model under security classification, *Discrete Dyn. Nat. Soc.*, **2017** (2017), 8609082. https://doi.org/10.1155/2017/8609082

26. S. Hosseini, M. A. Azgomi, The dynamics of an SEIRS-QV malware propagation model in heterogeneous networks, *Physica A*, **512** (2018), 803–817. https://doi.org/10.1016/j.physa.2018.08.081

27. L. Yang, X. Yang, Q. Zhu, L. Wen, A computer virus model with graded cure rates, *Nonlinear Anal. Real World Appl.*, **14** (2013), 414–422. https://doi.org/10.1016/j.nonrwa.2012.07.005

28. S. Lazfi, S. Lamzabi, A. Rachadi, H. Ez-Zahraouy, The impact of neighboring infection on the computer virus spread in packets on scale-free networks, *Int. J. Mod. Phys. B*, **31** (2017), 1750228. https://doi.org/10.1142/S0217979217502289

29. Y. Nath, K. K. Shukla, Retraction notice to: "Post-bucking of angle-ply laminated plates under thermal loading", *Commun. Nonlinear Sci. Numer. Simul.*, **126** (2023), 107442. https://doi.org/10.1016/j.cnsns.2023.107442

30. T. Li, Y. Guo, Optimal control and cost-effectiveness analysis of a new COVID-19 model for Omicron strain, *Physica A*, **606** (2022), 128134. https://doi.org/10.1016/j.physa.2022.128134

AIMS Press